Structural and Electronic Properties of Indium Phosphide Nanotubes

ARTICLE *in* THE JOURNAL OF PHYSICAL CHEMISTRY C · DECEMBER 2008

Impact Factor: 4.77 · DOI: 10.1021/jp8050438

2 AUTHORS:

Sudip Roy
CSIR - National Chemical Laboratory, Pune
41 PUBLICATIONS **386** CITATIONS
SEE PROFILE

Michael Springborg
Universität des Saarlandes
266 PUBLICATIONS **2,741** CITATIONS
SEE PROFILE

Article

Structural and Electronic Properties of Indium Phosphide Nanotubes

Sudip Roy, and Michael Springborg

J. Phys. Chem. C, **Article ASAP**

Structural and Electronic Properties of Indium Phosphide Nanotubes

Sudip Roy*,† and Michael Springborg*

Physikalische and Theoretische Chemie, Universität des Saarlandes, 66123 Saarbrücken, Germany

Received: June 9, 2008; Revised Manuscript Received: September 13, 2008

By use of a density-functional-based tight-binding method, indium phosphide (InP) nanotubes, which have been synthesized a few years ago, are studied computationally. Structural and electronic properties are calculated for two different types of structures, i.e., rolled, planar sheets and cylindrical cut-outs of the crystal. Both cases lead to stable structures of different diameter and thickness. In analyzing the results, we focus on structural relaxation, strain energy, Mulliken charge distributions, density of states, and HOMO−LUMO band gap as a function of tube diameter and thickness.

I. Introduction

Nanotubes and nanowires are ideal building blocks for nanoscale electronic and optoelectronic devices.[1] Following the identification of carbon nanotubes,[2] nanotubes, nanowires, and nanoribbons of several other materials have been synthesized and studied experimentally and theoretically, including MoS_2,[3,4] GaN,[5−8] AlN,[9−11] $AlGaN_2$,[12] boron,[13−15] $Mo_6S_{6-x}I_x$,[16,17] imogolite $[(HO)_3Al_2O_3SiOH]$,[18,19] and the material of the present study, InP,[20−23] although the experimentally studied systems often are thicker than those in theoretical studies. Compared to the crystalline materials, the electrons in nanotubes and nanowires are confined in two dimensions. Their properties can be modified in a more or less controllable way by varying material and/or the structure of the nanotube or nanowire. For semiconductors, the electronic properties also can be modified through n- or p-type doping.[24] Moreover, the nanowires can be modified by incorporating quantum dots into the wire.[25] For nanowires, the growth direction and the diameter provide two additional parameters that can be varied, whereas for nanotubes one has one further structural degree of freedom, i.e., both an inner (R_i) and an outer diameter (R_o) of the tube. Through their variation, it is possible to change the properties from those of nanowires (vanishing inner diameter) to those of rolled-up sheets (large inner and outer diameters, but small values of the thickness $t = R_o - R_i$.

Using the InP nanotubes that were synthesized some few years ago as an example, it is the purpose of the present contribution to analyze the dependence of the material properties on the diameters for nanowires and nanotubes. In particular we shall focus on stability, structure, and electronic properties. InP nanowires are extensively used in fiber optical communications, high-speed electronic applications, and optoelectrical devices. The increased quantum confinement for InP nanotubes compared to the nanowires makes InP nanotubes an interesting material for future semiconductor applications.

Like many other II−VI and III−V semiconductors, InP may crystallize in either the zinc blende or the wurtzite crystal structure. For crystalline InP the zinc blende structure is more stable than the wurtzite structure. However, very little is known about the structure of low-dimensional InP structures like, e.g., clusters, nanowires, and nanotubes. In a previous work we have examined the properties of stoichiometric and nonstoichiometric InP clusters without[26] and with passivating surfactants[27] using a density-functional tight-binding (DFTB) method.[28−30] The results suggested that the inner parts of the finite systems were structurally similar to those of the bulk but that noticeable deviations occur in the outer regions. Moreover, whether structures derived from the zinc blende or from the wurtzite crystal structure were the stabler ones was found to depend critically on the size of the clusters. We also found that the frontier orbitals have significant contributions from the surface regions.

According to experiments, the synthesized InP nanotubes have zinc blende-like structures, similar to the case for crystalline InP. The nanotubes are grown using vapor−liquid−solid (VLS) laser ablation. However, except for some structural characterization, very little is known about the properties of these nanotubes. In order to obtain a more detailed understanding of these materials, including understanding the differences between nanotubes on the one hand and clusters and the crystal on the other, we have carried out a thorough study of different structures of InP nanotubes and nanowires and shall here report the results of this study. This includes results on the stability, structure, and electronic properties for a large set of nanotubes, whereby diameters, thicknesses, and chiralities have been varied. In addition, we have studied structures obtained by rolling up a planar sheet of InP with an assumed graphene-like structure with, however, each In (P) atom surrounded by three P (In) neighbors. In all calculations we have used the above-mentioned DFTB method.

InP nanowires have been the subject of a couple of recent theoretical studies.[21,31,32] In two cases,[31,32] nanowires that were grown along the (111) direction were considered, whereas we here shall study nanowires along the (100) direction. In one earlier work the nanotubes were considered.[21]

The paper is organized as follows. Section II gives a brief description of the computational method, and our results are discussed in section III. Finally, our main conclusions are summarized in section IV.

II. Computational Procedure

The calculations were carried through using a parametrized density-functional tight-binding (DFTB) method that has been

* Corresponding authors: s.roy@theo.chemie.tu-darmstadt.de and m.springborg@mx.unisaarland.de.

† Present address: Eduard-Zintl-Institut für Anorganische and Physikalische Chemie, Technische Universität Darmstadt, Petersenstrasse 20, 64287 Darmstadt, Germany.

10.1021/jp8050438 CCC: $40.75

described in detail elsewhere[28−30] and, therefore, shall be only briefly described here.

We write the total energy of a given system relative to that of the isolated, noninteracting atoms as

$$E_b = \sum_i \epsilon_i - \sum_{jk} \epsilon_{jk} + \frac{1}{2}\sum_{k\neq l} U_{kl}(|\vec{R}_k - \vec{R}_l|) \quad (1)$$

Here, ϵ_i is the energy of the ith orbital for the system of interest and ϵ_{jk} is the energy of the jth orbital for the isolated kth atom. Moreover, U_{kl} is a pair potential between the kth and lth atom.

The Kohn−Sham single-particle operator is approximated as

$$\hat{h} = \hat{t} + V_{\text{eff}}(\vec{r}) = \hat{t} + \sum_j V_j^0(|\vec{r} - \vec{R}_j|) \quad (2)$$

with $\hat{t}$ being the kinetic-energy operator and $V_{\text{eff}}(\vec{r})$ being the effective Kohn−Sham potential that has been approximated as a superposition of the potentials of the neutral atoms.

The single-particle eigenfunctions $\psi_i(\vec{r})$ to the Kohn−Sham equations $\hat{h}\psi_i = \epsilon_i\psi_i$ are expanded in a set of atom-centered basis functions $\{\chi_{klm}(\vec{r})\}$. Here, k denotes the atom and (l, m) the angular dependence. By assuming that the matrix element $\langle\chi_{k_1l_1m_1}|V_j^0|\chi_{k_2l_2m_2}\rangle$ vanishes unless $k_1 = j$ and/or $k_2 = j$, the matrix elements $\langle\chi_{k_1l_1m_1}|\hat{h}|\chi_{k_2l_2m_2}\rangle$ and $\langle\chi_{k_1l_1m_1}|\chi_{k_2l_2m_2}\rangle$ can be obtained from density-functional calculations on the diatomic molecules. Finally, the pair potentials U_{kl} are determined so that parameter-free, density-functional binding-energy curves of the diatomics (i.e., in our case, In_2, P_2, and InP) are reproduced accurately.

In the present calculations the basis set consists of In 5s, 5p, and 5d functions as well as P 3s, 3p, and 3d functions, whereas all other occupied orbitals are treated within a frozen-core approximation. Since for the isolated atoms, In 4d functions lie about 5 eV below the P 3s orbitals, it may be suggested that the In 4d electrons should be treated explicitly. This would, however, lead to less flexibility of the basis set. In our earlier work on InP clusters[26] we showed that our approach gives accurate results for crystalline InP, making us confident that also the results for InP nanotubes will be accurate.

We considered two different types of structures. Although crystalline InP is formed from tetrahedrally coordinated atoms, we also considered rolled-up graphene-like sheets with 3-fold coordinated atoms. These structures have the advantage that no dangling bonds occur and have, moreover, been found relevant for nanotubes of similar materials like Si[33] and GaN.[5] Under special conditions also InP may take a graphene-like structure.[34] In order to ensure that graphene-like InP is at least metastable, we calculated the total energy of graphene-like InP and zinc blende-like InP as a function of the bond length. The results, Figure 1, show clearly that the zinc blende structure is more stable than the graphene structure but also that each structure separately is stable. There is also a noticeable difference in the lowest-energy nearest-neighbor distance. For the zinc blende this In−P bond length is 2.55 Å, whereas the graphene phase has a 6% smaller value. This is related to the sp^2 hybridization of InP in the graphene phase compared to the sp^3 hybridization for the zinc blende structure.

The rolling up of a graphene-like sheet of InP along a specific direction produces nanotubes that are similar to the carbon nanotubes.[2] Letting $\vec{a}$ and $\vec{b}$ be the lattice vectors of an infinite, two-dimensional honeycomb, the position of any hexagon is given through $n\cdot\vec{a} + m\cdot\vec{b}$ and, accordingly, uniquely defined through the two integers n and m.[35] These two integers define, subsequently, the nanotubes: upon rolling up the sheet the two hexagons at (0, 0) and (n, m) are mapped on top of each other. Two special cases are $n = m$, for which armchair nanotubes

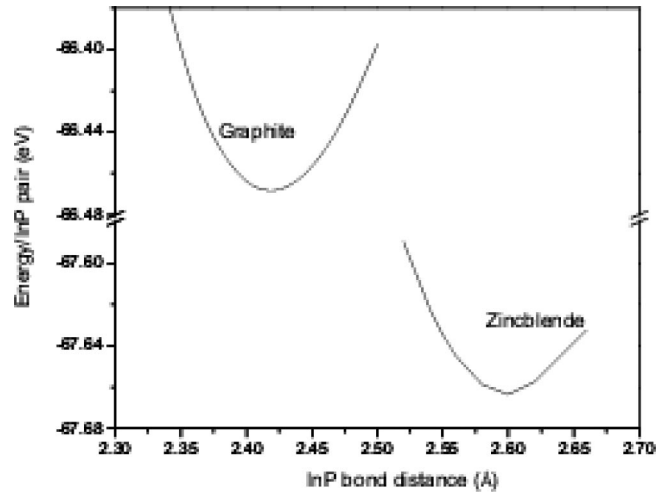

Figure 1. The total energy per InP pair for the zinc blende crystal and the graphene-like sheet as a function of nearest neighbor distance between In and P.

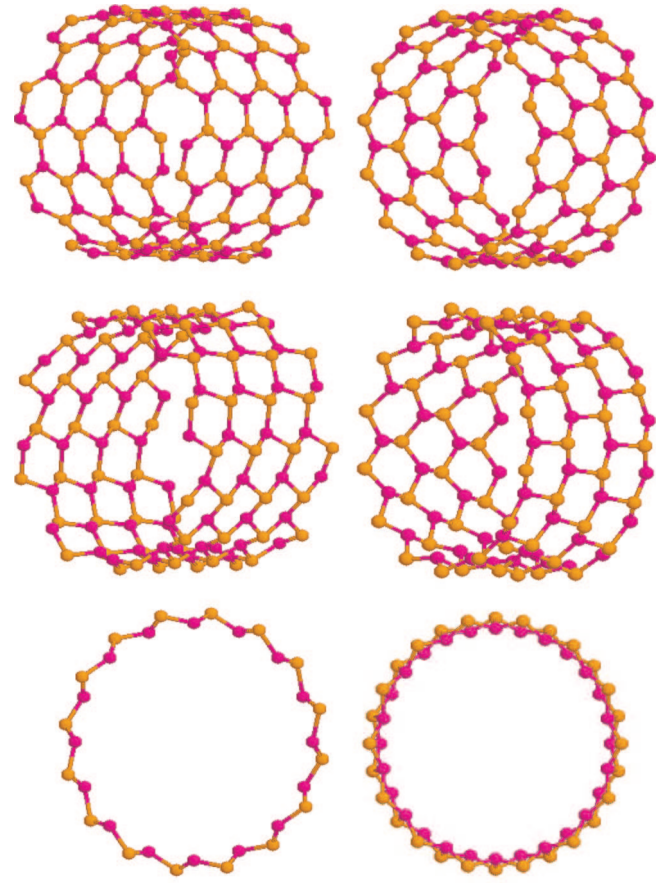

Figure 2. Initial (two top panels) and relaxed structures (four lower panels) of (left) (8, 8) and (right) (14, 0) single-wall nanotubes. Dark and light spheres represent P and In atoms, respectively.

result, and $m = 0$ resulting in zigzag nanotubes. An example of each type is shown in Figure 2. We performed calculations on (n, n) and $(n, 0)$ InP single-wall nanotubes (SWNTs) and double-wall nanotubes (DWNTs) as a function of n. We considered nanotubes with diameters ranging from 14 to 34 Å for armchair nanotubes and from 12 to 38 Å for zigzag nanotubes. Both the unit-cell length along the nanotube axis and all the internal structural degrees of freedom were optimized.

We shall let D be the diameter of the (unrelaxed) nanotube, q be the number of In−P atom pairs per repeated unit, and Q

TABLE 1: The Zinc Blende Derived Cylinders Studied in the Present Work.[a]

no.	(n_a, n_b)	R (Å)	q	Q
1	(0,0)	1.0	1	1
2	(0, −1), (−1, 0)	5.2	2	3
3	(0, 1), (1, 0)	6.6	2	5
4	(−1, −1)	7.3	1	6
5	(1, −1), (−1, 1)	8.4	2	8
6	(1, 1)	9.3	1	9
7	(0, −2), (−2, 0)	11.0	2	11
8	(−1, −2), (−2, −1)	12.1	2	13
9	(0, 2), (2, 0)	12.5	2	15
10	(1, −2), (−2, 1)	12.8	2	17
11	(2, −1), (−1, 2)	13.5	2	19
12	(2, 1), (1, 2)	14.1	2	21
13	(−2, −2)	15.6	1	22
14	(2, −2), (−2, 2)	16.6	2	24
15	(0, −3), (−3, 0)	16.9	2	26

[a] R is the radial distance from the outermost In and P atoms to the wire axis for the unrelaxed system, and q is the number of In−P atom pairs per repeated unit with that radial distance. Q is the total number of atom pairs per repeated unit. n_a and n_b give the values with the largest radial distances. A lattice constant of 5.87 Å was used.

be the total number of atoms per repeated unit. For the $(n, 0)$ tubes, $D = 3^{1/2}nd/\pi$ with d being the nearest-neighbor bond length in the graphene sheet. Moreover, $q = n$ for these structures. For the (n, n) tubes, $D = 3nd/\pi$ and $q = 2n$.

In addition, we considered the crystalline zinc blende structure and cut out a cylindrical shell with the common axis of the two cylinders parallel to the (001) direction. The axis was chosen so that it contains midpoints of In−P bonds, whereby stoichiometric nanotubes result with, moreover, the inner and outer surfaces both containing to equal parts In and P atoms. For the zinc blende crystal the atomic positions are given by

$$\pm(1,1,1)\frac{a}{8} + (n_a + n_b - n_c, n_a - n_b + n_c, -n_a + n_b + n_c)\frac{a}{2} \quad (3)$$

where a is the lattice constant, n_a, n_b, and n_c are integers, and the + (−) sign is used for In (P) atoms. The distances for the atoms with a z coordinate equal to $\pm a/8$ to the z axis (which we will call the radial distances) are given by

$$R = \left[{n_a}^2 + {n_b}^2 + \frac{1}{32} \pm (n_a + n_b)\frac{1}{4}\right]^{1/2} a \quad (4)$$

Using $a = 5.87$ Å, we obtained the cylinders that are listed in Table 1. These initial structures were allowed to relax to their nearest local total-energy minimum. For these systems we shall use a notation extracted from Table 1. Thus, the (14, 6) nanotube was constructed as the cylinder for which all atoms have initial radial distances between 6 and 14 au, i.e., 3.2 and 7.4 Å, and which, accordingly, has 6 − 1 = 5 InP atom pairs per unit cell.

Both types of structures are periodic along the z axis. We shall use a supercell approach with about 20 unit cells per supercell but then only $k = 0$ in the Brillouin zone sampling.

III. Results and Discussion

A. Nanotubes Derived from Graphene-like Structures. At first we consider a strain energy, defined as the energy difference between the tube and an infinite, periodic graphene-sheet-like structure; i.e., it is the energy needed for making a tube from the sheet. This energy is shown in Figure 3 for the zigzag and armchair InP SWNT. From the figure it is evident that the zigzag

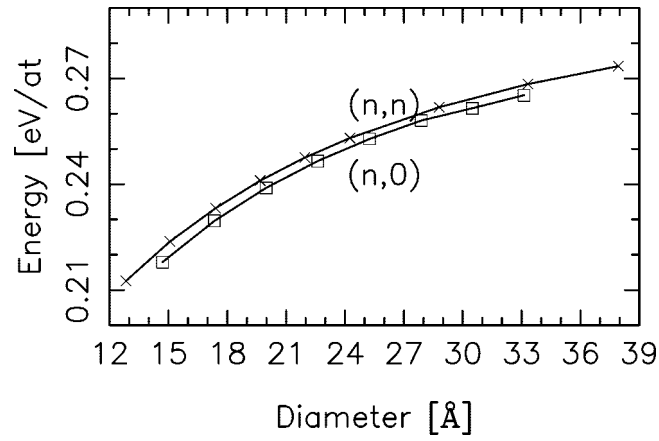

Figure 3. The strain energy as a function of tube diameter for (squares) $(n, 0)$ and (crosses) (n, n) single-wall nanotubes. Results are shown for the (5, 5), (6, 6), (7, 7),..., (10, 10), (12, 12), (14, 14), (16, 16) and the (10, 0), (12, 0),..., (24, 0) nanotubes.

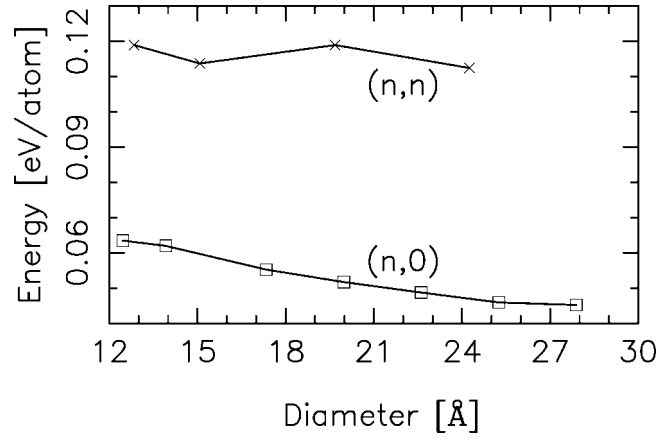

Figure 4. The strain energy as a function of the outer tube diameter for double-wall nanotubes. The squares mark double-wall nanotubes with tubes $(n, 0)$ and $(n + 4, 0)$ for $n = 4, 6,...,$ and 16, whereas the crosses mark those for (n, n) and $(n + 4, n + 4)$ for $n = 1, 2, 3,$ and 5.

$(n, 0)$ SWNTs are less stable than the armchair (n, n) SWNTs. A surprising result is that the strain energy is an increasing function of diameter in the size range we have studied. Ultimately, for very large diameters, the strain energy should approach 0. This finding is different from the results for carbon, phosphorus,[36] and gallium nitride[5] nanotubes but is similar to what has been found for SiH nanotubes[33] for which all the hydrogen atoms are attached to the outer surface layer. A possible explanation is that an increased diameter leads to an increased bond angle away from the optimal value of 109.5° for tetragonally coordinated atoms. This also explains why it was not possible to fit each of the two curves in Figure 3 with a function of the form $a_1/D^{z_1} + a_2/D^{z_2}$ which ultimately could be used in estimating that value of D for which the strain energy has its maximum. However, when the results of Figure 3 are due to orbital interactions, their functional dependence on D is complicated. This also means that we are not able to estimate the value of D for which the strain energy reaches its maximum.

Our InP SWNTs contain dangling bonds on the surface instead of H atoms. One may, therefore, suggest two approaches for stabilizing these nanotubes, i.e., either saturating the dangling bonds by some ligands or adding an extra layer, leading to DWNTs. Actually, the experimentally studied systems are considerably thicker than SWNTs. Here, we constructed DWNTs by adding another layer of InP with the same chirality and,

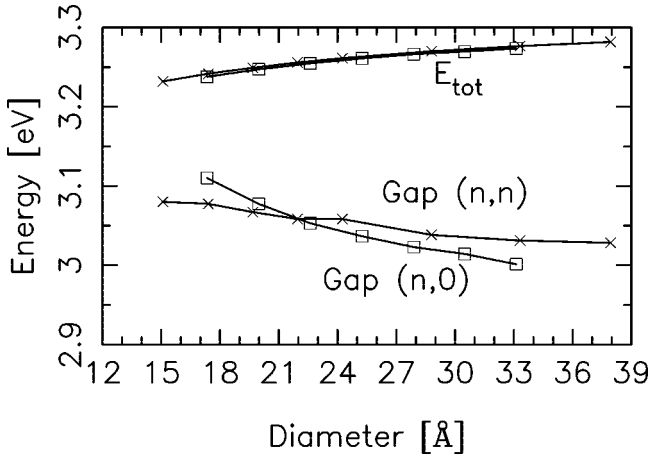

Figure 5. The HOMO−LUMO gap (lower curves) and the total energy per atom, shifted by a constant (upper curves), as a function of the tube diameter for (squares) $(n, 0)$ and (crosses) (n, n) single-wall nanotubes. Results are shown for the (5, 5), (6, 6), (7, 7),..., (10, 10), (12, 12), (14, 14), (16, 16) and the (10, 0), (12, 0),..., (24, 0) nanotubes.

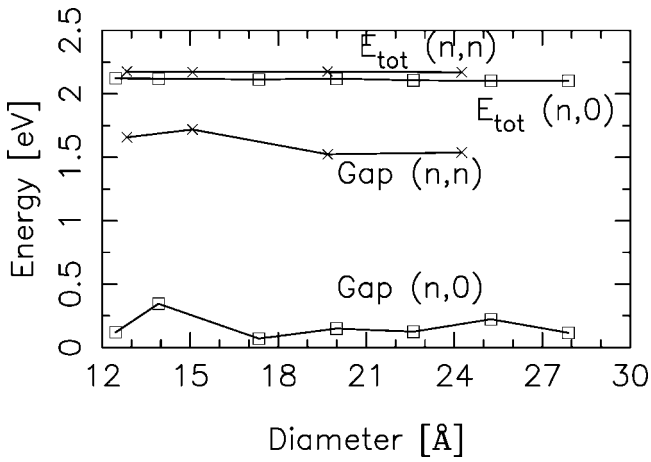

Figure 6. The HOMO−LUMO gap (lower curves) and the total energy per atom, shifted by a constant (upper curves), as a function of the outer tube diameter for double-wall nanotubes. The squares mark double-wall nanotubes with tubes $(n, 0)$ and $(n + 4, 0)$ for $n = 4, 6,...,$ and 16, whereas the crosses mark those for (n, n) and $(n + 4, n + 4)$ for $n = 1, 2, 3,$ and 5.

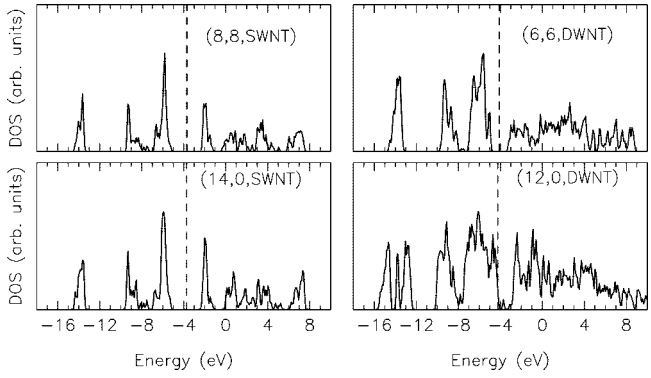

Figure 7. Density of states for different single- and double-wall nanotubes. The vertical, dashed line marks the Fermi energy.

subsequently, relaxed the whole system. To keep the thicknesses largely fixed for all the double-wall nanotubes, we have considered pairs of SWNTs of the form $(n, 0)$ and $(n + 4, 0)$ for the zigzag nanotubes and (n, n) and $(n + 4, n + 4)$ for the armchair ones.

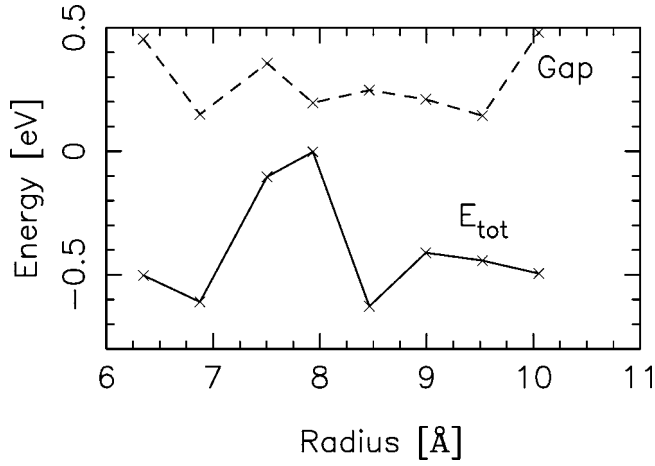

Figure 8. (Full curve) variation of the total energy per InP pair as well as (dashed curve) the HOMO−LUMO energy gap, both as a function of the outer radius of the relaxed nanotube for zinc blende-derived nanotubes. The thickness of the unrelaxed structure has been kept fixed at 4.76 Å.

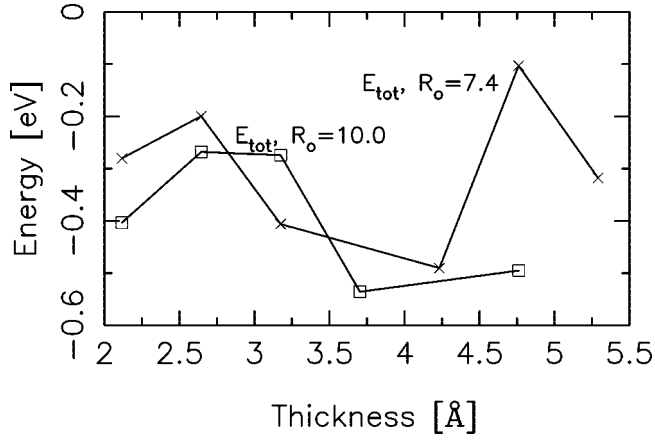

Figure 9. Variation of the total energy per InP pair as a function of the thickness of the nanotube for zinc blende-derived nanotubes. The outer radius was set equal to (squares) 10 Å and (crosses) 7.4 Å.

As shown in Figure 4, the resulting structures indeed are considerably more stable than the SWNTs. Moreover, the strain energy no longer possesses the atypical behavior as a function of nanotube diameter that was observed in Figure 3. The figure also shows that the (n, n) DWNTs are more stable than the $(n, 0)$ DWNTs.

In Figure 2 we show the relaxed and unrelaxed structure for one single example of the SWNTs. The buckling of the structure, which clearly can be recognized in the figure, is further evidence of the tendency of InP to adapt structures that resemble those of tetrahedrally coordinated atoms. The nearest-neighbor bond length is 2.54 Å which is similar to the bond length of 2.55 Å of crystalline InP with the zinc blende structure but larger than the value for the infinite, planar graphene-like sheet. The bond angle of In−P−In is about 107° for (n, n) and 109° for $(n, 0)$ nanotubes, respectively, which is very similar to the values for a tetrahedral geometry. This, again, suggests that the structural relaxation results in a structure that is approaching that of zinc blende.

We shall now turn to the electronic properties of the SWNTs and DWNTs. In Figures 5 and 6 we show the band gap of these two sets of nanotubes. In contrast to our earlier results on InP clusters,[26,27] the band gap between the highest occupied and lowest unoccupied orbitals (HOMO and LUMO, respectively)

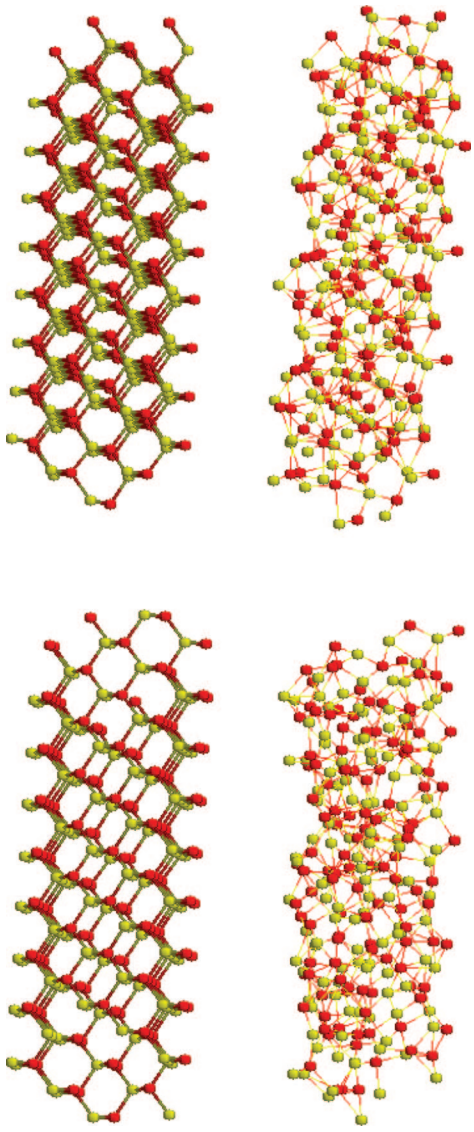

Figure 10. The (left panels) initial and (right panels) relaxed structures of the (upper panels) (13, 4) and (lower panels) (14, 6) zinc blende-derived nanotubes.

is here a smooth function of the size of the system. In our earlier studies we observed a close correlation between the HOMO−LUMO gap and the stability. The fact that both properties showed a rather irregular behavior as a function of system size could be related to differences in the structure of the surface, since at least one of the HOMO and LUMO was localized to the surface region. In the present case for the SWNTs and DWNTs the surface does not change markedly as a function of size of the system, which can explain why both the total energy and the gap are smooth functions of system size. Figure 5 shows also that larger $(n, 0)$ SWNTs have larger band gap than (n, n) SWNTs and that there is a crossover for diameters slightly above 20 Å. Passing to the DWNTs, the HOMO−LUMO gap drops drastically, being just slightly above 0 for the (n, n) DWNTs.

In Figure 7 we show the density of states for different SWNTs and DWNTs. Here, the bands from −16 to −12 eV are due to the 3s functions of phosphorus, those from −10 to −5.5 eV are formed by 3p functions of P, and the higher-lying bands are due to 5s and 5p of In. The individual features in the density of states are in general broader for the DWNTs than for the SWNTs which suggests that their widths may be used in estimating the thickness of InP nanotubes.

The only other study on this type of system, the semiempirical study on finite InP nanotubes by Erkoç,[21] gave HOMO−LUMO band gaps of 2.6−3.3 eV, i.e., close to our values. Erkoç considered just two structures of each type of nanotube, i.e., armchair and zigzag ones, but found that armchair nanotubes were more stable than zigzag nanotubes, again in agreement with the results of our study.

B. Nanotubes Derived from Zinc Blende Structures. From the results of the preceding subsection it is clear that the SWNTs are, at best, metastable and DWNTs adopt a structure that has many features in common with that of crystalline zinc blende InP, including partial tetrahedral coordination of the atoms. Therefore, we have also considered nanotubes which are generated from the zinc blende crystal structure. We generate these tubes with different diameter and thickness by cutting hollow cylinders from the bulk structure of InP, as described in section II.

In Figure 8 we show the variation in the total energy for those structures as a function of the radius of the outer cylinder. The figure shows a much less regular behavior of the total energy than we have found above for the SWNTs and DWNTs and, moreover, the occurrence of particularly stable structures (for 7 and 8.5 Å). The strong variation in the total energy can be related to the number of outermost (surface) atoms; cf. Table 1. In general, structures with few surface atoms are more stable than those with more surface atoms.

The total-energy variations in Figure 8 are much larger than those we found for the graphene-derived structures, which may be related to a much less regular surface structure for the structures of the present subsection. Moreover, the most stable zinc blende-derived structures are more stable than any of the single- or double-wall nanotubes of the preceding subsection, but alternatively, the less stable zinc blende-derived structures are less stable than the SWNTs and DWNTs. In this figure we also show the HOMO−LUMO gap. This is seen to be significantly smaller than the values we have found for most of the SWNTs and DWNTs. Moreover, no correlation between gap and stability is observed.

As can be seen in Figure 9, also through variation of the thickness of the nanotube, structures of particular stability can be obtained. Experimentally it has been observed that the more

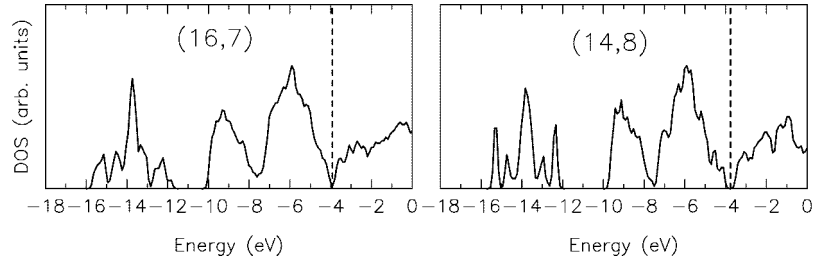

Figure 11. The density of states for two zinc blende-derived nanotubes. The vertical, dashed line marks the Fermi energy.

stable nanotubes have thicker walls with a morphology of the zinc blende structure.[20]

For the thinnest systems, it turns out that the structural relaxation leads to structures for which the hollow part is essentially eliminated; i.e., the structure changes from that of a nanotube to that of a nanowire. This is seen in Figure 10. Only when the hollow part is sufficiently large will the system remain hollow.

The Mulliken gross populations on the individual atoms as a function of their distances to the chain axis can be used in analyzing a possible spatial charge transfer. It turns out that there is an electron transfer from In to P and, in some cases, a weak tendency for an increased transfer near the outer surface, but this tendency is not as pronounced as we have found earlier for InP clusters.[26]

The density of states for these nanotubes, Figure 11, shows an overall agreement with the ones of Figure 7, although in particular the gap around the Fermi level is smaller for the zinc blende-derived nanotubes than for the graphene-derived ones. Moreover, when the two curves in Figure 11 are compared in more detail, the HOMO−LUMO gap is larger for the (14, 8) nanotube than for the (16, 7) one; i.e., of those two, the one with the larger gap is the more stable one (cf. Figure 8), a correlation between gap and stability that is equivalent to what we have found for clusters.

In their theoretical study on (111)-derived InP nanowires for which dangling bonds on the surface have been saturated with H atoms, Schmidt et al.[31] found that the stability of the systems is a monotonically increasing function of radius. This confirms our suggestion that the irregular behavior of the total energy as a function of radius, Figures 8 and 9, indeed is due to dangling bonds at the surface. This also suggests that the systems we have considered here can be stabilized through surfactants. Indeed, Leitsmann and Bechstedt[32] recently demonstrated that the stability of various III−V semiconductor nanorods was governed by their surface.

IV. Conclusions

Using a parametrized, density-functional, tight-binding method, we have calculated structural and electronic properties of InP nanotubes with different diameter, thickness, and chirality. Our work is the first theoretical study of such different types of InP nanotubes generated from two types of crystal structures.

Our main conclusions are as follows. (a) Single-wall nanotubes with large diameters are less stable due to dangling bonds on the surface and an unfavorable value of the angle between these dangling bonds and an In−P bond (i.e., $\ll 109°$). (b) Adding an extra layer, thereby obtaining a double-wall nanotube and removing some of the dangling bonds, results in an increased stability, which is larger for systems with larger diameter. (c) For both single- and double-walled systems the tube relaxes toward a structure with increased similarity with the zinc blende crystal structure. (d) The double-wall nanotubes are semiconductors with a small band gap independently of chirality and structure. (e) The single-wall nanotubes have larger band gaps. (f) The most stable nanotubes are obtained from the zinc blende crystal structure. (g) For those there is a nontrivial dependence of stability on diameter and thickness of the nanotube. (h) This irregular behavior is dictated by the surfaces of the nanotubes.

Acknowledgment. This work was supported by the Deutsche Forschungsgemeinschaft (DFG) through the SFB 277 at the Universität des Saarlandes.

References and Notes

(1) Hu, J.; Odom, T. W.; Lieber, C. M. *Acc. Chem. Res.* **1999**, *32*, 435.
(2) Lijimi, S.; Ichihashi, T. *Nature* **1993**, *363*, 603.
(3) Seifert, G.; Terrones, H.; Terrones, M.; Jungnickel, G.; Frauenheim, T. *Phys. Rev. Lett.* **2000**, *85*, 146.
(4) Tenne, R.; Homyonfer, M.; Feldman, Y. *Chem. Mater.* **1998**, *10*, 3225.
(5) Li, S. M.; Lee, Y. H.; Hwang, Y. G.; Elsner, J.; Porezag, D.; Frauenheim, T. *Phys. Rev. B* **1999**, *60*, 7788.
(6) Carter, D. J.; Gale, J. D.; Delley, B.; Stampfl, C. *Phys. Rev. B* **2008**, *77*, 115349.
(7) Xu, B.-S.; Zhai, L.-Y.; Liang, J.; Ma, S.-F.; Jia, H.-S.; Liu, X.-G. *J. Cryst. Growth* **2006**, *291*, 34.
(8) Simpkins, B. S.; Ericson, L. M.; Stroud, R. M.; Pettigrew, K. A.; Pehrsson, P. E. *J. Cryst. Growth* **2006**, *290*, 115.
(9) Zhao, M.; Xia, Y.; Zhang, D.; Mei, L. *Phys. Rev. B* **2003**, *68*, 235415.
(10) Tondare, V. N.; Balasubramanian, C.; Shende, S.; Joag, D. S.; Godbole, V. P.; Bhoraskar, S. V. *Appl. Phys. Lett.* **2002**, *80*, 4813.
(11) Wu, Q.; Hu, Z.; Wang, X.; Lu, Y.; Chen, X.; Xu, H.; Chen, Y. *J. Am. Chem. Soc.* **2003**, *125*, 10176.
(12) Pan, H.; feng, Y. P.; Lin, J. *J. Chem. Theory Comput.* **2008**, *4*, 703.
(13) Tang, H.; Ismail-Beigi, S. *Phys. Rev. Lett.* **2007**, *99*, 115501.
(14) Singh, A. K.; Sadrzadeh, A.; Yakobson, B. I. *Nano Lett.* **2008**, *8*, 1314.
(15) Xu, T. T.; Zheng, J.-G.; Wu, N.; Nicholls, A. W.; Roth, J. R.; Dikin, D. A.; Ruoff, R. S. *Nano Lett.* **2004**, *4*, 963.
(16) Popov, I.; Yang, T.; Berber, S.; Seifert, G.; Tománek, D. *Phys. Rev. Lett.* **2007**, *99*, 085503.
(17) Vrbanić, D.; Remškar, M.; Jesih, A.; Mrzel, A.; Umek, P.; Ponikvar, M.; Jančar, B.; Meden, A.; Novosel, B.; Pejovnik, S.; Venturini, P.; Coleman, J. C.; Mihailović, D. *Nanotechnology* **2004**, *15*, 635.
(18) Guimaraes, L.; Enyashin, A. N.; Frenzel, J.; Heine, T.; Duarte, H. A.; Seifert, G. *Nano* **2007**, *1*, 362.
(19) Cradwick, P. D.; Wada, K.; Russell, J. D.; Yoshinag, N.; Masson, C. R.; Farmer, V. C. *Nat. Phys. Sci.* **1972**, *140*, 187.
(20) Bakkers, E. P. A. M.; Verheijen, M. A. *J. Am. Chem. Soc.* **2003**, *125*, 3440.
(21) Erkoç, Ş. *J. Mol. Struct. (THEOCHEM)* **2004**, *676*, 109.
(22) Novotny, C. J.; Yu, E. T.; Yu, P. K. L. *Nano Lett.* **2008**, *8*, 775.
(23) Novotny, C. J.; DeRose, C. T.; Norwood, R. A.; Yu, P. K. L. *Nano Lett.* **2008**, *8*, 1020.
(24) Haraguchi, K.; Katsuyama, K.; Hiruma, K.; Ogawa, K. *Appl. Phys. Lett.* **1992**, *60*, 745.
(25) Björk, M. T.; Ohlsson, B. J.; Thelander, C.; Persson, A. I.; Deppert, K.; Wallenberg, L. R.; Samuelson, L. *Appl. Phys. Lett.* **2002**, *81*, 4458.
(26) Roy, S.; Springborg, M. J. *Phys. Chem. B* **2003**, *107*, 2771.
(27) Roy, S.; Springborg, M. *J. Phys. Chem. A* **2005**, *109*, 1324.
(28) Blaudeck, P.; Frauenheim, Th.; Porezag, D.; Seifert, G.; Fromm, E. *J. Phys.: Condens. Matter* **1992**, *4*, 6389.
(29) Porezag, D.; Frauenheim, Th.; Köhler, Th.; Seifert, G.; Kaschner, R. *Phys. Rev. B* **1995**, *51*, 12947.
(30) Seifert, G.; Porezag, D.; Frauenheim, Th. *Int. J. Quantum Chem.* **1996**, *58*, 185.
(31) Schmidt, T. M.; Miwa, R. H.; Venezuela, P.; Fazzio, A. *Phys. Rev. B* **2005**, *72*, 193404.
(32) Leitsmann, R.; Bechstedt, F. *J. Appl. Phys.* **2005**, *102*, 063528 (
(33) Seifert, G.; Köhler, Th.; Urbassek, H. M.; Hernández, E.; Frauenheim, Th. *Phys. Rev. B* **2001**, *63*, 193409.
(34) Gallium Nitride. *Semiconductors and Semimetals*; Pankova, J. I., Moutakas, T., Eds.; Academic Press: New York, 1998; Vol. 50.
(35) Hamada, N.; Sawada, S.; Oshiyama, A. *Phys. Rev. Lett.* **1992**, *68*, 1579.
(36) Cabria, I.; Mintmire, J. W. *Europhys. Lett.* **2004**, *65*, 82.

JP8050438